La^{3+} and Y^{3+} interactions with the carboxylic acid moiety at the liquid/vapor interface: identification of binding complexes, charge reversal, and detection limits.

Adrien Sthoer,[a] Ellen M. Adams,[b] Sanghamitra Sengupta,[a] Robert Corkery,[a,c] Heather C. Allen,[b] and Eric C. Tyrode*[a]

[a]*Department of Chemistry, KTH Royal Institute of Technology, SE-10044 Stockholm, Sweden*

[b]*Department of Chemistry & Biochemistry, The Ohio State University, Columbus, Ohio 43210, USA.*

[c]*Department of Applied Mathematics, Research School of Physics and Engineering, Australian National University, Canberra, ACT0200, Australia*

* Corresponding author: Email: tyrode@kth.se

Abstract

Specific interactions of yttrium and lanthanum ions with a fatty acid Langmuir monolayer were investigated using vibrational sum frequency spectroscopy (VSFS). The trivalent ions were shown to interact with the charged form of the carboxylic acid group from nanomolar concentrations (<300 nM). Analysis of the spectral features from both the symmetric and the asymmetric carboxylate modes reveals the presence of at least three distinct coordination structures linked to specific binding configurations. Although the same species were identified for both La^{3+} and Y^{3+}, they display a different concentration dependence, highlighting the ion-specificity of the interaction. From the response of interfacial water molecules, charge reversion, as well as the formation of yttrium hydroxide complexes, were detected upon increasing the amount of salt in the solution. The binding interaction and kinetics of absorption are sensitive to the solution pH, showing a distinct ion speciation in the interfacial region when compared to the bulk. Changing the subphase pH or adding a monovalent background electrolyte that promotes deprotonation of the carboxylic acid headgroup, could further improve the detection limit of La^{3+} and Y^{3+} to concentrations <100 nM. These findings demonstrate that nM concentrations of trace metals contaminants, typically found on monovalent salts, can significantly influence the binding structure and kinetics in Langmuir monolayers.

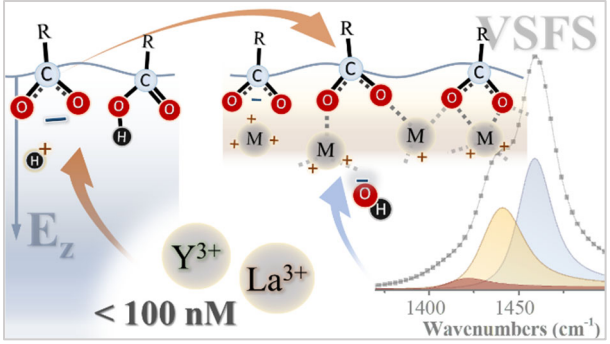

1. Introduction

The binding of transition metal ions to charged surfaces is vital in many processes, such as protein folding,[1] atmospheric chemical reactions,[2] and geochemical sequestration and transport of contaminants already from sub-micromolar concentrations.[3] A multitude of studies have demonstrated the ion specific nature of surface binding phenomena, in which ions with the same charge can interact and subsequently alter monolayer properties in different manners.[4-11] Long chain fatty acids have been used as a model for negatively charged surfaces to investigate the cation binding due to the prevalence of carboxylic acid groups in biological and atmospheric chemistry systems.[12-14]

Grazing incidence X-ray diffraction (GIXD) measurements and spectroscopic studies of metallic soaps have been combined in an attempt to correlate the coordination structures of the carboxylate moiety with its vibrational signatures and the ion-specific nature of the metallic cations.[15-17] Similar investigations have been carried out for hydrated carboxylate anions in aqueous solution.[18] However, less is known about coordination structures of metallic cations to carboxylates constrained at interfaces, especially for polyvalent ions. Existing studies of carboxylate interfaces report contrasting results and interpretations for the type of binding interactions.[19-23] This is especially true in the case of monovalent and divalent salts, where strong discrepancies were observed in the vibration frequency of the metal-carboxylate complex, which could vary with time, even for highly concentrated solutions.[22, 24, 25]

While differences in experimental parameters, such as pH, could account for some of these observed discrepancies, recent studies by Sthoer et al. has revealed that a trace amount of polyvalent ions in solution can compete with the ion of interest for adsorption sites and cause variations in the vibrational pattern of the fatty acid monolayer.[26] While the impact of organic impurities included in the salts used had been previously demonstrated,[24, 27] the latter study showed that trace amounts of polyvalent metal impurities, such as trivalent ions, must also be considered when investigating binding to a charged interface.[26]

Studies of trivalent cation binding are challenging due to the limitations in predicting their speciation in aqueous solutions and their complex electronic structures. Nevertheless, trivalent ions are known to play a central role in proteins and colloidal reactivity, being held responsible for crystallization phenomena, phase separation and surface charge reversion.[28-30] For example, the adsorption of Fe^{3+} and La^{3+} on bacterial and bovine serum albumin proteins was revealed to be strongly pH dependent at micromolar concentrations,[31, 32] and caused a charge reversion of lipid surfaces starting from sub-micromolar $LaCl_3$ concentrations.[33, 34]

The complexation of trivalent ions La^{3+} and Fe^{3+} to the specific carboxylic acid of a fatty acid monolayer has been probed by X-ray reflectivity, X-ray fluorescence, and more recently VSFS.[35-38] Specific ion effects were observed, in which it was concluded that La^{3+} adsorption to the carboxylic acid was led only by Coulombic interactions. On the other hand, the interaction of Fe^{3+} was determined to be of a covalent nature, depending on the solution pH as iron hydroxide complexes readily form.[35, 36] VSFS investigations in millimolar concentrations confirmed the ion specificity and pH dependence of the ionic interactions in the OH water region; however, little attention was brought to the direct molecular interactions with the carboxylic acid headgroup, the charge reversion and the co-ions binding.[38] To the

authors' knowledge, no molecular observations have been reported for Y^{3+} ion interactions with the fatty acid Langmuir monolayer.

In this study VSFS is used to probe the complexation of trivalent ions to an arachidic acid (AA) Langmuir monolayer. La^{3+} and Y^{3+} were chosen as they both possess an accommodating speciation diagram in the pH range where the carboxylic acid headgroup deprotonates. Moreover, they interact through their *s* electrons' shell, which gives a spherical symmetry and a large flexibility to form similar coordinated complexes despite their difference in size. Additionally, these ions are of interest as they are frequently present as impurities in some salts and used in microelectronics and the newest hydrides technologies.[39, 40] We find that the binding interaction is concentration dependent and specific to each cation. The deprotonation of the carboxylic acid at natural pH begins at concentrations as low as 300 nM. This detection limit is further decreased to 100 nM by adding a NaCl background electrolyte, which promotes the binding of Y^{3+}. The interfacial water response is also systematically compared with the carboxylate binding pattern. It reveals to be more sensitive to the first stages of deprotonation, as well as the charge reversal of the monolayer at higher ionic strengths. Furthermore, ion adsorption kinetics are found to be impacted by changes in the subphase pH. Taken together, these results demonstrate that trivalent ions have specific spectroscopic signatures that could be used to identify trace metal contaminants in solutions, and that ion speciation as a function of pH and adsorption kinetics must be considered in diffusion-limited cation binding investigations.

2. Experimental section

2.1. Materials. YCl_3 (99.99%, trace metals basis, anhydrous), $LaCl_3.(H_2O)_7$ (99.999%, trace metals basis), NaCl (99.999%, trace metals basis), NaOH (99.99%, trace metals basis), eicosanoic-d39 acid (97%, dAA for deuterated arachidic acid), eicosanoic acid (99% AA for arachidic acid), and chloroform (anhydrous grade, stabilized with ethanol) were obtained from Merck. HCl 36.5% (99.999%, trace metals basis) was purchased from Alfa-Aesar. Ultrapure water was obtained from an Integral 15 Millipore system with a resistivity of 18.2 MΩ.cm and a total organic content < 3 ppb. NaCl was baked at 500°C for 1h to remove potential traces of organic compounds. All other compounds were used as received. The glassware was cleaned by a three-step sonication procedure, first in ethanol, followed by an alkaline cleaning agent solution (Deconex from Borer Chemie), and finally, ultrapure water. The glassware was thoroughly rinsed in ultrapure water between each step. In order to avoid ionic specific interactions at the surface of the pH sensor glass electrode, the pH was adjusted prior to the addition of salt and later cross-checked with multiple pH paper indicators (MColorpHast™ pH 0 – 14, 4.0 – 7.0, 6.5 – 10, and 11.0 – 13.0 and Whatman® Panpeha™ pH 0 – 14 from Merck).

2.2 Fatty acid compression isotherms. The compression isotherms and VSF spectroscopy measurements on the fatty acid monolayers were carried out in a temperature-controlled trough (KSV NIMA, 50 mm width, 9,750 mm^2) made out of Teflon™ with Delrin™ compression barriers. The surface pressure was measured with a 10 mm wide Wilhelmy paper plate. Fatty acid depositing solutions were prepared in chloroform. The spectroscopy measurements were performed no less than 10 min after the deposition of the monolayer to ensure the evaporation of the solvent. The temperature of the subphase was kept constant at 22°C ±0.1°C. The trough

was carefully cleaned before every experiment and soaked overnight with a saturated solution of EDTA to remove any potential traces of trivalent ions from previous experiments (~3 mM at 25°C). The EDTA procedure was found to be an important step to ensure reproducible results, particularly at sub μM concentrations, as evidence was found that yttrium and lanthanum cations could adsorb (or maybe even absorb) to the Teflon trough. All SF spectroscopy measurements presented in this article were performed at a constant surface pressure of 20 mN/m.

2.3. Vibrational Sum Frequency Spectroscopy. The VSF spectrometer has been described in detail elsewhere.[41] Briefly, a fraction of the output from a Ti:Sapphire amplifier (~90 fs, 1 kHz, ~6 W, Integra-C, Amplitude Technologies, France) is used to pump a HE-Topas (Light Conversion, Lithuania), to obtain a broadband tunable IR pulse. The remaining fraction of the amplifier output is sent to a home-built pulse shaper, to generate a bandwidth tuneable 805 nm picosecond pulse. The visible and IR beams are focused on the sample position in a co-propagating geometry at angles of incidence of 70° and 55°, and average powers of ~30 mW and ~4 mW, respectively. The setup displays a high degree of automation, which allows collecting spectra in wide spectral regions. The spectral resolution in these experiments was set to < 3 cm^{-1} by closing the slit in the beam shaper. Spectra were recorded in the three polarization combinations, mainly SSP, SPS, and PPP, and normalized by the non-resonant SF response from a gold surface.[41] To quantify the deprotonation of the monolayer, as well as the respective contributions of the metal-carboxylate complexes, the spectra were fitted with a convolution of Lorentzian and Gaussian line shapes, which account respectively for homogeneous and inhomogeneous broadening (see SI for additional details).[42, 43] All the SF spectra are presented in normalized units (n.u.) using as reference the r^+ mode in the SSP spectrum of arachidic acid on a pure water subphase.

3. Results and Discussion

3.1. Surface pressure (Π) vs. molecular area (A) isotherms: effect of Y^{3+} and La^{3+}

Langmuir isotherms of arachidic acid (AA) on YCl_3 and $LaCl_3$ solutions were recorded for concentrations varying from 100 nM up to 1 mM. Figure 1 shows the Π-A isotherms for four selected concentrations of YCl_3, as well as that for a pure water subphase. For concentrations below 1 μM YCl_3 the isotherms are largely similar to that on pure water, displaying three distinct regions: a coexistence region between a 2D gas (G) and a tilted condensed (TC) phase at molecular areas > ~24 $Å^2$, a purely TC phase, and an untilted condensed (UC) phase at surface pressures above ~27 mN/m.[44-47] At 1 μM YCl_3 changes become apparent in the isotherm, with the TC-UC phase transition pressure decreasing to ~20 mN/m. At 10 μM the TC phase is no longer present, leaving the 2D gas phase in direct equilibrium with a UC phase. Further increasing the salt concentration leads to a small expansion of the monolayer with the appearance of a non-horizontal plateau starting from a surface pressure of $\pi_t \approx 3$ mN/m at 100 μM, and the replacement of the 2D gas coexistence region by a liquid expanded (LE) phase. Finally, at 1 mM YCl_3 no discontinuities are apparent in the isotherm, showing a continuous transition between the LE and UC phase at the highest surface pressures. The π-A isotherms of AA on $LaCl_3$ solutions show a very similar concentration dependent behaviour (see SI).

The surface equilibria described by the Langmuir isotherms reflect a subtle balance between cohesive and repulsive forces. The former include short range Van der Waals interactions between the alkyl chains, headgroup bridging through hydrogen-bonding, and complex formation, while the latter refers to short and long range forces opposing the packing, such as steric overlap, electrostatic repulsion between charged headgroups, as well as diffusion and thermal motion.[44, 48-51] The contraction of the monolayer to the densest UC phase reflect an increase of the cohesive forces, as observed, for example, in stearic acid monolayers interacting with divalent ions at high concentrations.[52] On the contrary, monolayer expansion and appearance of the plateau of phase transition with a LE phase, result from the introduction of new repulsive forces, which in the case of fatty acid monolayers on monovalent chloride salt solutions originate from the charging of the monolayer.[53, 54] The Langmuir isotherms recorded for YCl_3 and $LaCl_3$ indicate that the interfacial equilibrium is affected in both ways, revealing a complex interaction between the trivalent ion salts and the carboxylic acid headgroup. A molecular insight into these interactions is revealed by vibrational sum frequency spectroscopy.

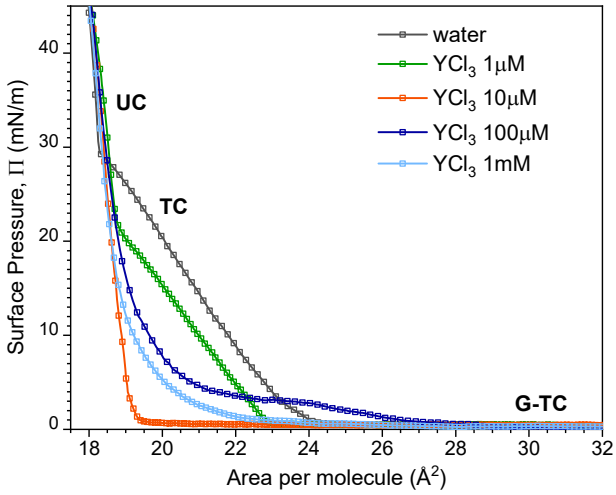

Figure 1. Surface pressure vs. molecular area isotherms of an arachidic acid monolayer on a pure water subphase and different YCl_3 concentrations. pH ~5.8 and temperature 22°C. The phases in equilibrium depicted (UC, TC, and G) correspond to those of the pure water subphase. Equivalent isotherms for $LaCl_3$ can be found in the SI.

3.2. Y^{3+} and La^{3+} interactions with the carboxylate headgroup: concentration dependence

The SF spectra of dAA Langmuir monolayers on solutions of varying concentrations of YCl_3 and $LaCl_3$ under the SSP polarization combination are shown in Figures 2a and 2b. The spectral region shown targets vibrational modes from the deuterated alkyl chain and the carboxylic acid headgroup. In the CD stretching region, the three sharp peaks centered at ~2075 cm^{-1}, ~2135 cm^{-1}, and ~2218 cm^{-1}, are all linked to the terminal methyl group and assigned to the symmetric (r^+), Fermi resonance (r^+_{FR}), and asymmetric stretches (r^-), respectively.[47, 55] The lack of features associated with the CD_2 groups indicate that the alkyl chain has a high degree of conformational order, consistent with the high packing density in the monolayer in an all-trans configuration. The vibrational modes from the chain appear

insensitive to increasing amounts of trivalent ions in solution, and the phase transition between the tilted to untilted condensed phases (TC→UC). This is rationalized by the similar area per molecule expected at 20 mN/m for all salt concentrations (see Figure 1).

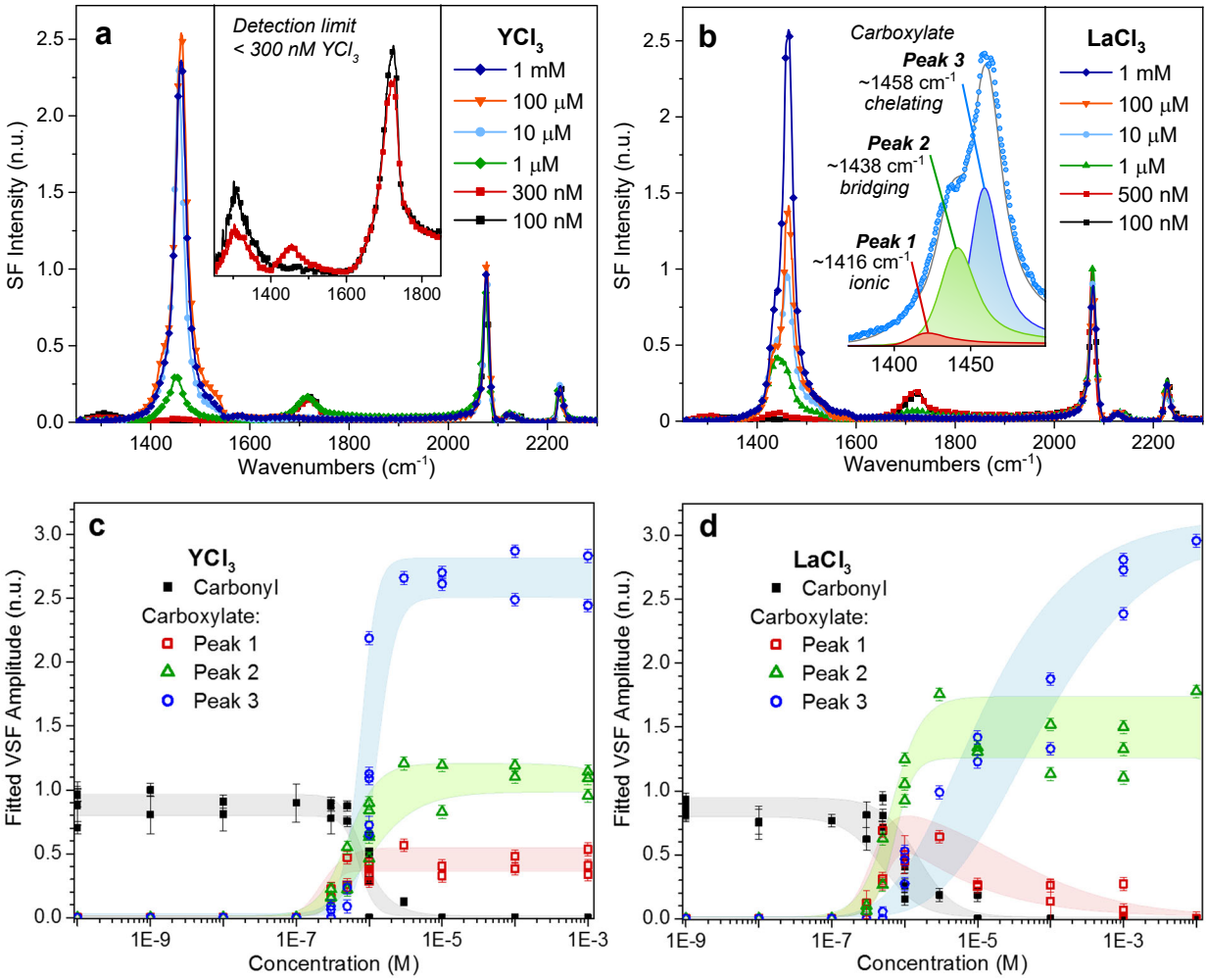

Figure 2. VSF spectra recorded under the SSP polarization combination of a dAA Langmuir monolayer on an aqueous subphase containing 100 nM up to 1 mM of a) YCl_3 and b) $LaCl_3$ at pH ~5.8. The surface pressure was set to 20 mN/m and the temperature to 22°C. In the inset in b) three contributions can be distinguished for the carboxylate symmetric modes that are associated with specific metal-carboxylate coordination structures: ionic (Peak 1), bridging bidentate (Peak 2), and chelating bidentate (Peak 3)(assignment are discussed in a later section). c) Fitted amplitudes for the three carboxylate peaks and carbonyl stretch as a function of YCl_3 and d) $LaCl_3$ concentration. Shaded regions are added as guides to the eyes to distinguish the trends for the different peaks.

In contrast, significant changes are observed in the headgroup vibrations. Up to ~100 nM, the spectra look similar to that of pure water, where only features from the uncharged carboxylic acid headgroup are detected, mainly the broad C-OH stretch at ~1300 cm^{-1}, and the carbonyl stretch C=O at ~1720 cm^{-1} (see inset in Figure 2a).[47] However, starting from 300 nM, the deprotonation of the monolayer becomes apparent for both YCl_3 and $LaCl_3$ with the appearance of carboxylate stretching modes between 1400 – 1500 cm^{-1}. This sets the detection limits for Y^{3+} and La^{3+} in the range between 100 and 300 nM.

Further increasing the salt concentration in the subphase leads to multiple vibrational contributions in the carboxylate region, as well as the decrease of the C=O mode from the

uncharged carboxylic acid. Three resolved features can be readily identified in the symmetric carboxylate stretching region. They are centered at approximately ~1416 cm^{-1} (*Peak 1, ionic*), ~1438 cm^{-1} (*Peak 2, bridging bidentate*), and ~1458 cm^{-1} (*Peak 3, chelating bidentate*), as shown in the inset in Figure 2b. The same modes are observed for lanthanum and yttrium, but their relative intensities and concentration dependence vary depending on the identity of the cation. Though the assignments will be discussed in more detail in the next section, it is assumed that each symmetric carboxylate stretching contribution corresponds to a defined ion-pair or binding configuration between the metallic cation and the carboxylate.

The relative changes are better visualized in Figures 2c and 2d, where the fitted amplitudes for the three symmetric carboxylate peaks, as well as that for the carbonyl stretch, are shown as a function of ion concentration. The figures summarize the results from multiple repeat experiments (see SI for details of the fitting procedure). The C=O signal for both salts starts decreasing at sub μM concentrations and is no longer present at 10 μM, indicating that the monolayers are fully deprotonated beyond this point (the apparent binding constants for pK_Y and pK_{La} are both 6.0±0.1). This is in stark contrast to the predictions of the Gouy Chapman model for 1:3 salts, which concludes that the monolayer should be ~10% deprotonated at 10 μM and just ~25% at 1 mM (see SI). This adds support for strong specific interactions between the trivalent cations and the carboxylic acid group, which are not accounted for in the Poisson-Boltzmann theory. Moreover, the absence of the hydrated carboxylate symmetric stretch at ~1408 cm^{-1}, which has been observed in fatty acid monolayers on solutions containing monovalent ions that do not specifically interact with the carboxylate,[26, 47] show that complex formation occurs from the lowest trivalent ion concentrations.

Focusing on the amplitudes of the symmetric carboxylate peaks, the trends for the yttrium cation show a typical Langmuir behaviour for all the three contributions, where saturation levels are reached at ~5 μM (Figure 2c). On the contrary, for the bulkier lanthanide, a steady-state in the binding configuration is only reached at 10 mM, with two carboxylate contributions (*Peak 1* at ~1416 cm^{-1} and *Peak 3* at ~1458 cm^{-1}) showing opposite trends once the monolayer is fully deprotonated (Figure 2d). These contrasting behaviours demonstrate differences in the binding mechanisms as well as the binding-pattern proportions between the two cations. Given that the cross-sections for each species are not known with sufficient precision, the absolute proportions between the different complexes in the monolayer cannot be accurately determined. However, a rough estimate is proposed in the SI.

3.3. Interfacial binding patterns: assignment of the carboxylate stretching modes

The identification of the type of coordination from the vibrational frequencies of the carboxylate stretches relies on previous correlations established by comparison with crystallographic structures in solid-state acetate crystals,[15, 56] and in aqueous acetate solutions.[18] The relevant parameters to consider are the centre positions of the symmetric and asymmetric stretching modes ($\nu_{coo-,s}$, $\nu_{coo-,as}$), and their relative difference in frequencies $\Delta(\nu_{as} - \nu_s)$. However, it has been recognized that additional factors could influence the vibrational pattern observed. They include the polarity of the metal-oxygen bonds, the identity of the cation, the geometry of the O-C-O angles, or even the number of water molecules interacting with the charged species.[15, 18, 57] Despite these limitations, a general classification, albeit with many exceptions, has been proposed for $\Delta(\nu_{as} - \nu_s)$, where $\Delta_{Unidentate}$

> Δ_{Ionic} > $\Delta_{Bridging/Chelating}$ with $\Delta_{Chelating}$ (< 90 cm^{-1}) often < $\Delta_{Bridging}$.[16, 58] The typical coordination possibilities between metal cations and the carboxylate group are depicted in Figure 3. Except for the ionic / ion-pair form that results from electrostatic interactions,[59] the metal-carboxylate coordinative binding complexes are commonly sorted into four distinct classes, namely unidentate (I), chelating bidentate (II), bridging bidentate (III), and polymeric/tridentate forms (IV).[15, 17, 56] The polymeric form is a mixture between the chelating and bridging bidentate, where at least one of the oxygen atoms is simultaneously coordinated to two metallic cations, which in turn can also be involved in a type (II) or type (III) binding with another carboxylate group.[15, 17]

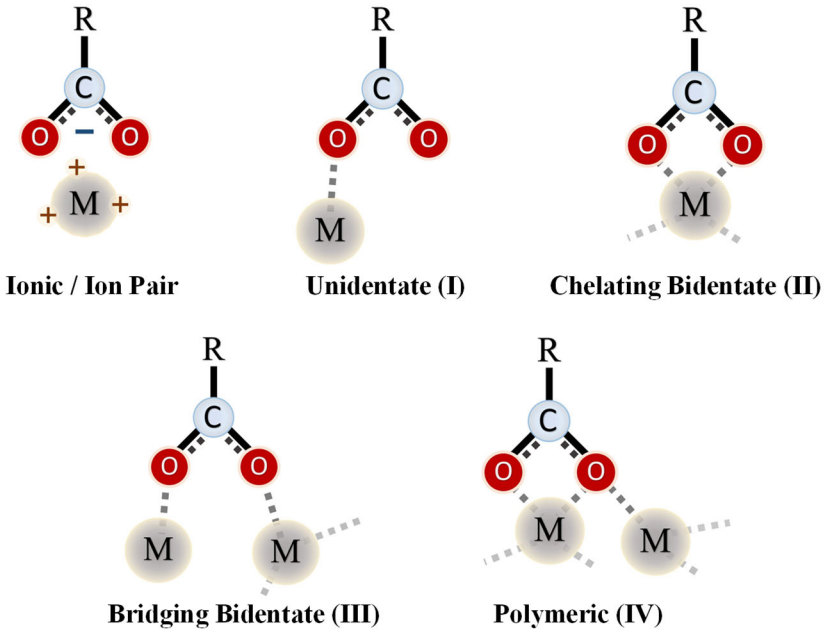

Figure 3. Schematic representation of the typical coordination modes for the carboxylate group with metallic cations.

As shown in the previous section, in VSFS, the symmetric stretches are predominantly observed under the SSP polarization combination. The asymmetric carboxylate stretches are, in turn, mainly detected in the SPS polarization, with PPP spectra showing contributions from both. Spectra recorded in the three polarization combinations for dAA monolayers on 1 mM YCl_3 and $LaCl_3$ subphases are presented in Figure 4. Besides the symmetric carboxylate stretches previously described for the SSP spectra, in the SPS spectra, several resolved features are observed at higher frequencies. Assigned to asymmetric stretches, they are centered at ~1520 cm^{-1} *(Peak 4)*, ~1540 cm^{-1} *(Peak 5),* and ~1575 cm^{-1} *(Peak 6)*. In the inset of Figure 4b, where an enlarged view of the SPS and PPP spectra is presented for $LaCl_3$, the contributions from the three symmetric and the three asymmetric modes can be clearly resolved. The average peak positions for the six bands obtained from the fits of all spectra collected are summarized in Table 1.

Each symmetric carboxylate mode should have an associated asymmetric band; however, the pairing is not entirely obvious given the number of features observed. The assignment of

Peak 1 at ~1416 cm^{-1} is the most straightforward, as it lies in the frequency range of ion pairing interactions (solvent-shared /contact ion pairs) with the carboxylate headgroup.[26, 54] Thus, in agreement with Marcus et al. classification, it arises from pure electrostatic interactions and likely associated with a solvent separated ion pair with the hydrated trivalent ion.[59] Based on the same studies,[26, 54] the accompanying asymmetric stretch for *Peak 1* is expected between 1535 and 1540 cm^{-1}, but with an order of magnitude lower intensity. Consequently, given the relatively weak amplitude of *Peak 1* (Figure 2c and 2d), its asymmetric stretch should be barely detectable and, if anything, contributing to the intensity of *Peak 5*.

Table 1. Vibrational frequencies of the symmetric $\nu_{coo-,s}$ *and asymmetric* $\nu_{coo-,as}$ *stretches of the carboxylate headgroup of the arachidic acid monolayers on* YCl_3 *and* $LaCl_3$ *subphases.*

	Symmetric $\nu_{coo-,s}$			**Asymmetric $\nu_{coo-,as}$**		
	Peak 1 (ionic)	*Peak 2 (bridging)*	*Peak 3 (chelating)*	*Peak 4 (chelating)*	*Peak 5 (bridging)*	*Peak 6* (weak)
YCl_3	1416±1cm^{-1}	1437±2 cm^{-1}	1457±3 cm^{-1}	1525±5 cm^{-1}	1545±5 cm^{-1}	1577±3 cm^{-1}
$LaCl_3$	1416±1 cm^{-1}	1438±1 cm^{-1}	1459±3 cm^{-1}	1523±3 cm^{-1}	1545±5 cm^{-1}	1577±3 cm^{-1}

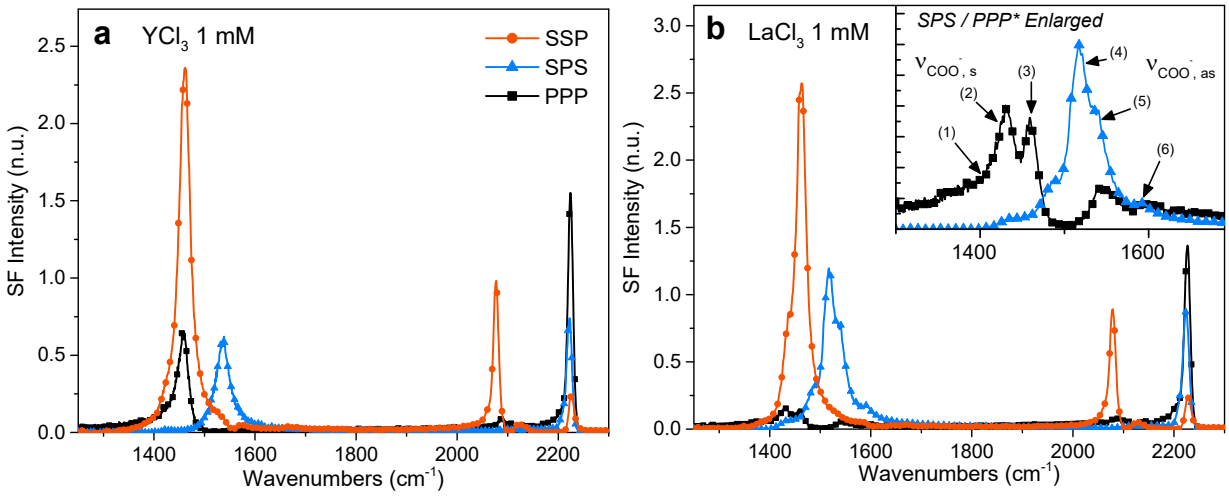

Figure 4. VSF spectra recorded under the SSP, SPS and PPP polarization combinations of dAA monolayers on a) 1mM YCl_3 *and b) 1mM* $LaCl_3$ *solution at pH ~5.8. The inset b) is an enlargement of the SPS and PPP spectra, where the PPP* spectrum has been multiplied by 5 for ease of comparison.*

The asymmetry stretches linked to *Peak 2* at ~1438 cm^{-1}, and *Peak 3* at ~1458 cm^{-1}, can be determined by comparing the evolution of their fitted amplitudes as a function of salt concentration with those from the asymmetric stretches, particularly in the case of $LaCl_3$ where the two bands are more readily resolved. It is concluded that *Peak 2* is associated with *Peak 5* at ~1545 cm^{-1} and *Peak 3* with *Peak 4* at ~1525 cm^{-1} (see SI for an extended description of this procedure). The *Peak 2-Peak 5* symmetric/asymmetric correlation is also further supported by previous studies on Mn^{2+} and Ni^{2+} interactions with carboxylic acid monolayers, where single bands linked to the symmetric and asymmetric stretches were observed at equivalent peak positions. Nonetheless, the symmetric pair for the weak

asymmetric contribution at ~1577 cm^{-1} (*Peak 6*) remains uncertain (possibly linked to the polymeric complexes). The proposed assignments for both trivalent salts are summarized in Table 2. The chelating bidentate coordination (II) (*Peak 3 – Peak 4*) exhibiting a particularly short frequency difference $\Delta(\nu_{as} - \nu_s) \approx 60$ cm^{-1} is predominant for the two salts at high concentrations, followed by the bridging bidentate coordination (III) (*Peak 2 – Peak 5*). The presence of both bridging and chelating complexes suggests that polymeric structures (IV) involving several carboxylate headgroups also form at the surface.

Table 2. Proposed assignments of the interfacial binding pattern for yttrium and lanthanum – carboxylate complexes.

$\nu_{coo-,s} - \nu_{coo-,as}$	$\Delta(\nu_{as} - \nu_s)$	**Coordination mode**
Peak (1) – Peak (5)	≈ 130 cm^{-1}	Ionic (ion pair)
Peak (2) – Peak (5)	≈ 100 cm^{-1}	Bridging bidentate (III)
Peak (3) – Peak (4)	≈ 60 cm^{-1}	Chelating bidentate (II)

Previous studies on specific interactions of lanthanum and yttrium ions with the carboxylate moiety in the bulk had suggested similar types of complexes. For instance, a combined X-ray, IR, and NMR study on hydrated acetate crystals proposed bridging and polymeric complexes for La^{3+}, and polymeric and chelating complexes for Y^{3+}.[60] Another study using Raman spectroscopy targeting C-C stretching modes for determining the interactions of lanthanum with a hydrated lithium acetate, suggested the coexistence of both bridging and chelating bidentate structures, with a predominance of the chelating bidentate over the polymeric form.[61] However, many such studies in solid state or aqueous bulk solution are not directly transposable to the Langmuir monolayers. Given that the fatty acid monolayer is packed at the air/water interface, the possible carboxylate configurations and their respective interactions with trivalent cations are necessarily constrained. The stress added to the interfacial configuration (angles, distance, and strength of the chemical bonds) may induce variation in the frequency of vibration.

To confirm the assignments proposed for the planar geometry, a comparison is made with the lamellar bilayer structures of rare earth metallic soaps, for which single crystalline structures have been determined.[62-65] When the alkyl chain of the metallic soaps is four carbons or longer, their configurations are similar to that of the all-trans hexagonal packing of the fatty acid in the UC phase. From the published crystalline structure of lanthanum butyrate monohydrate,[63] which is almost identical to that of the neodymium butyrate,[62] we examine in Figure 5 the cross-section of the lamellar structure in the constrained environment of the monolayer. Both the chelating and bridging bidentate complexes can be readily identified (Figure 5b), which is consistent with the assignments from the SF spectra. The crystal structures from metallic soaps also provide an insight into the differences observed between La^{3+} and Y^{3+}. The yttrium cation has a coordination number (C.N.) of 8,[66] compared with a C.N. of 9 [63] for the lanthanum ion that is also 20% larger, [67] which provides the latter more flexibility to coordinate with neighbouring carboxylates via bridging complexes (note that a maximum of 6 carboxylate-oxygens can coordinate to the cations in the monolayer, with the remaining sites occupied by water-oxygens). Given that in Figure 5 one of the butyrate layers in the lamella

was removed from the originally electrically neutral soap structure, the case shown would correspond to a charge overcompensated monolayer with a 2 (La^{3+}) : 3 (COO^{-}) ratio. Overcharging is indeed observed for the highest salt concentrations, as discussed in the following section when evaluating the response from the OH stretching modes. However, at lower salt concentrations, when the monolayer charge is compensated in a 1:3 ratio, fewer ions will be present at the surface and the preferred binding complex will depend on the identity of the ion. A coarse analysis of how the trivalent ion will arrange at the surface for the charge compensated case in a packed carboxylic acid monolayer is presented in the SI (Figure S7).

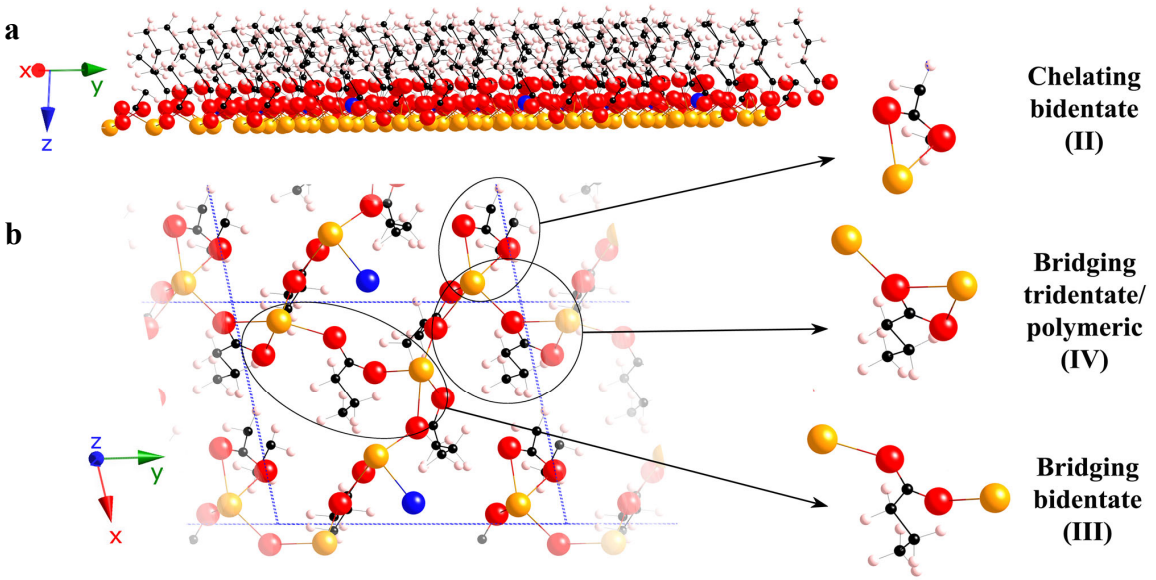

Figure 5. Single monolayer extracted from the crystal structure of lanthanum(III) butyrate monohydrate presented along the (a) z-y plane and the (b) x-y plane. In the structure seen in the xy plane (b), several carboxylate coordination structures with the La^{3+} can be identified, mainly chelating bidentate, bridging bidentate, and bridging tridentate (polymeric). They are consistent with the structure derived from the SF spectra of arachidic acid Langmuir monolayers. In the figure, yellow spheres represent La^{3+} ions, red spheres carboxylate oxygens, and blue spheres selected water oxygens. The small black and white spheres are carbon and hydrogen atoms, respectively.

3.4. Targetting interfacial water molecules to detect the charge reversion of the surface

The OH stretching bands from interfacial water molecules can be sensitive probes for detecting changes in the surface charge. The bands report both on water molecules in direct proximity to the monolayer, as well as those found further into the bulk within the diffuse double layer that are perturbed by the decaying surface electric field.[68, 69] The SSP polarized VSF spectra of AA monolayers on varying concentrations of YCl_3 in the subphase are presented in Figure 6. Equivalent spectra for pure water and 1 mM NaCl are also added for reference.[47] The two broad bands centered at ~3250 cm^{-1} and ~3500 cm^{-1} on the pure water spectrum primarily originate from H_2O molecules directly interacting with the uncharged carboxylic acid headgroup.[47, 70] In the pure water case, contributions from molecules in the diffuse double layer are negligible (the Debye screening length in pure water is significantly longer than the

non-linear coherence length of the SF process, and most of the signal from the diffuse double layer cancels due to destructive interference[68, 71]).

Upon addition of 100 nM YCl_3 to the subphase the OH bands increase relative to those of pure water (Figure 6). The added intensity results primarily from water molecules in the diffuse layer, and is a direct indication of the onset of the monolayer deprotonation (Gouy-Chapman model predicts ~3% deprotonation, see SI). The water bands are thus more sensitive probes than the carboxylate stretching modes to detect the first stages of charging (Figure 2a, COO^- features are below the detection limit at 100 nM). At 1 µM YCl_3, when the monolayer is roughly 50% deprotonated (see C=O amplitude in Figure 2c) and the Debye screening length is ~2 times shorter, the OH contributions decrease below those from pure water. Had the surface charged been proportional to the amount of unprotonated carboxylic acid groups, the water signal would have at least of the same order of magnitude as the one observed for 1 mM NaCl (Figure 6). The discrepancy shows that yttrium cations not only promote deprotonation but upon adsorption and complexation with the carboxylate, they also reduce the net surface charge. By further increasing the salt concentration, the water bands reach close to zero intensity at 10 µM YCl_3, before increasing again at higher concentrations, but with a broadband centered this time at ~3150 cm^{-1} and a sharper feature at ~3670 cm^{-1}.

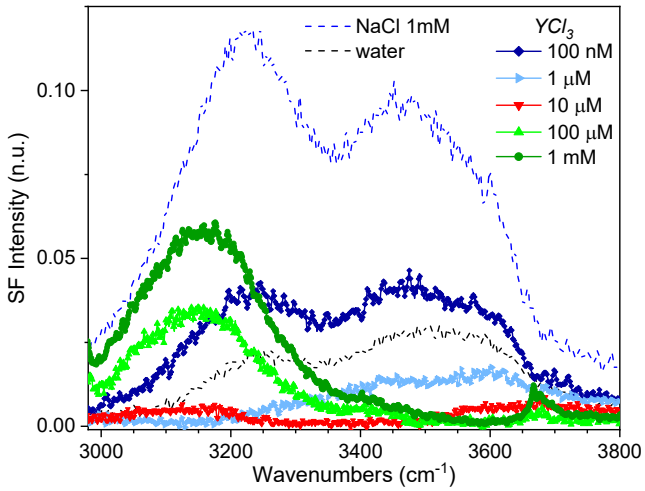

Figure 6. VSF spectra in the OH stretching region of perprotonated AA monolayers on solutions containing increasing concentrations of YCl_3. Spectra were recorded under the SSP polarization combination at pH ~5.8 and 22 °C. Equivalent spectra on 1 mM NaCl and pure water are also added for reference.

The trend involving a decrease of SF intensity to a minimum, followed by an increase and a red-shift of the main contributing broad, is indicative of a reversion of the surface charge, from negative to positive. This effect has been previously observed in several systems undergoing charge inversion, such as when adsorbing the positively charged CTAB surfactant on a negatively charged silica/water interface,[72] and at the TiO_2/water[73] and CaF_2/water[74, 75] interfaces when varying the solution pH, among many other examples.[28, 34] The charge reversion or overcompensation is typically driven by specific interactions of multivalent counterions with surfaces that display a relatively high charge density.[76-78] For the case of yttrium (and lanthanum), this strong interaction is demonstrated by the formation

of binding complexes with the carboxylate headgroup, as revealed by VSFS. The behaviour is also consistent with the changes observed in the surface pressure isotherms as a function of salt concentration (Figure 1), where the most compressed monolayer is seen at 10 μM YCl_3, the concentration where charge neutralization is approximately reached.

The relatively sharp feature observed at ~3670 cm^{-1} provides additional support for the charge inversion at high YCl_3 concentrations. The high-frequency band is located in a similar frequency range as that observed for the OH stretches of Si-OH, Al-OH, and Ca-OH at the aqueous interface with silica,[43, 79] alumina,[80] and calcium fluoride,[81] respectively. Thereby, it is assigned to the OH stretch of an yttrium hydroxide cation (i.e. $Y(OH)_2^+$ or $Y(OH)^{2+}$). The change in sign of the surface potential due to charge overcompensation causes a significant increase in the concentration of surface anions, including OH^-, which can interact with the Y^{3+} ions already present at the surface. This will be further discussed in the next section.

3.5. Role of the surface charge on the surface speciation and detection limit

YCl_3 as well as $LaCl_3$ show relatively intricate speciation diagrams at basic pH, with the formation of several hydroxide complexes, as shown in Figure 7a for the yttrium case. Up to pH ~7, the prevalent species is the free ionic form Y^{3+}. However, further increasing the pH shows the appearance of YOH^{2+}, $Y(OH)_2^+$, and $Y(OH)_{3(s)}$, at the expense of the free ion. Conversely, below pH 6, when only the pH determining ions are present in solution, the fatty acid monolayer is uncharged, but deprotonates in more alkaline conditions, reaching approximately 50% deprotonation at pH~ 10.8.[47] All VSF measurements discussed above were recorded at pH~5.8, where yttrium and lanthanide are in their free ionic form (i.e. Y^{3+} and La^{3+}), and the fatty acid monolayer is at the deprotonation threshold (i.e., it can start to deprotonate even by the addition of small amounts of monovalent salts to solution).[47] To explore the influence of the bulk speciation as well as the intrinsic deprotonation state of the monolayer on the type of binding complex formed, measurements were carried out at several different pH at a constant concentration of 1 μM YCl_3. The corresponding VSF spectra recorded under the SSP polarization are shown in Figure 7b.

The spectrum at pH ~5.8 is similar to that presented in Figure 2a for 1 μM YCl_3, where the principal band in the symmetric carboxylate stretching region is centered at ~1458 cm^{-1}, and assigned to the chelating bidentate complex (marked as *ii* in Figure 7b). The spectral features at the other measured pH show, however, significant differences. At pH 5, when the yttrium ion is in its free ionic form Y^{3+} but the monolayer does not as easily deprotonate, besides a weak broadband centered at ~1455 cm^{-1} (*ii*), the spectrum shows a sharp contribution at ~1475 cm^{-1} (*i*). This latter band was not observed at pH ~5.8 at any salt concentration for either YCl_3 or $LaCl_3$, and indicates that lowering the pH favours a different type of yttrium-carboxylate coordination pattern. When increasing the pH to 8, the main component in the symmetric carboxylate band is similar to that at pH ~5.8 (*ii*), but with a much lower intensity. The formation of $YOH^{2+}$and $Y(OH)_2^+$ at the expense of Y^{3+} in the bulk, clearly has an influence as the hydroxides do not as readily interact with the carboxylate headgroup. At pH 9, there is only a very small indication of monolayer deprotonation, despite the fact that in the absence of trivalent ions the monolayer should be ~20% deprotonated.[47] Given that at pH 9 $Y(OH)_{3(s)}$

is the main species and that almost all yttrium should precipitate out from solution, the effect observed must be caused by trace amounts of trivalent soluble species. Finally, at pH 11 when most yttrium is found in the trihydroxide form, a strong symmetric carboxylate stretch is seen at ~1408 cm^{-1}, which correspond to the hydrated or solvent separated carboxylate, typically observed for monovalent ions.[26, 47] Consequently, no traces of yttrium are detected with regards to the vibrational pattern of the carboxylate. However, the deprotonation fraction of the monolayer is lower than expected at this pH,[47] revealing residual metal-carboxylate interactions as developed below. All these results show that the speciation of yttrium in the bulk solution has, as expected, a strong influence on the observed behaviour. The formation of hydroxide complexes reduces the charges carried with the ionic yttrium species and the global amount of ionic species available, at the same time decreasing their propensity to migrate to the surface.

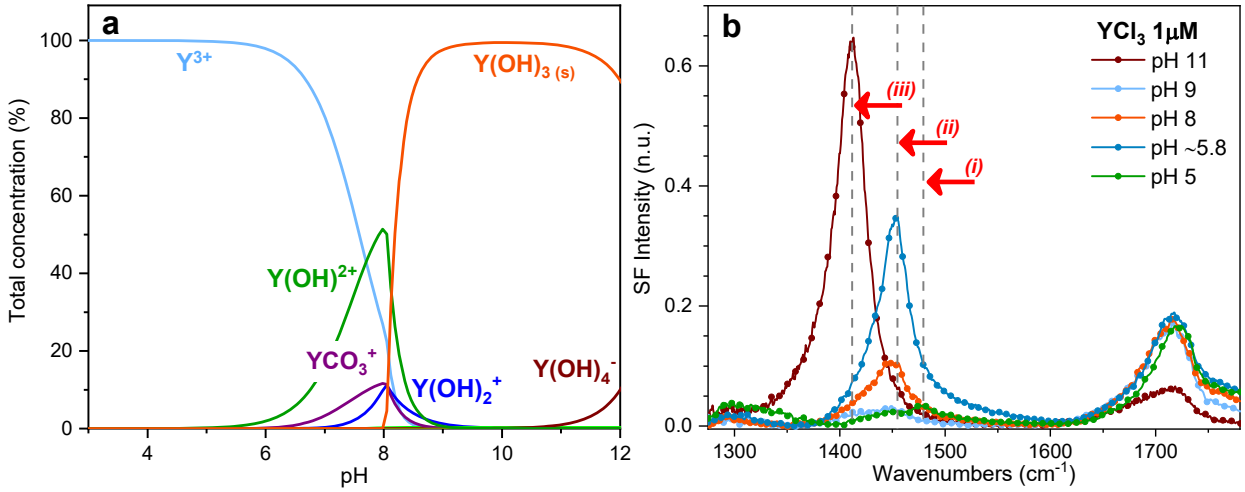

Figure 7. a) Speciation diagram of YCl_3 at 25°C calculated from HYDRA and MEDUSA software for a concentration of 1 µM dissolved CO_2 (see SI for the full diagram). b) SSP polarized VSF spectra of dAA on YCl_3 1 µM electrolyte solutions at pH 5, ~5.8, 8, 9 and 11 adjusted with either HCl, or NaOH. The spectra were collected 10 min after the deposition of the monolayer (time ="0").

Time dependence: All data presented in Figure 7b were recorded 10 minutes after the deposition of the monolayer on the electrolyte subphase (referred to as time "0"). However, in the pH range where the Y^{3+} was not the dominant species, the spectra exhibited some time dependence. Figure 8 shows spectra of the fatty acid monolayer at pH 9 and pH 11 collected at different times after deposition. Whereas at pH 9 almost no traces of deprotonation are detected at time = 0, the monolayer appears to almost fully deprotonate 40 minutes later, with a sharp peak centered at ~1459 cm^{-1}, characteristic of the chelating binding pattern with yttrium ions. Similarly, at pH 11, the hydrated carboxylate contribution at 1408 cm^{-1} decreases at t = +90 min, while a shoulder at ~1458 cm^{-1} appears in the spectra. For both cases, the interaction of trivalent ions with the interface becomes obvious with time. It is worth noting that no such time dependence was observed in the spectra presented in the previous sections collected at pH ~5.8.

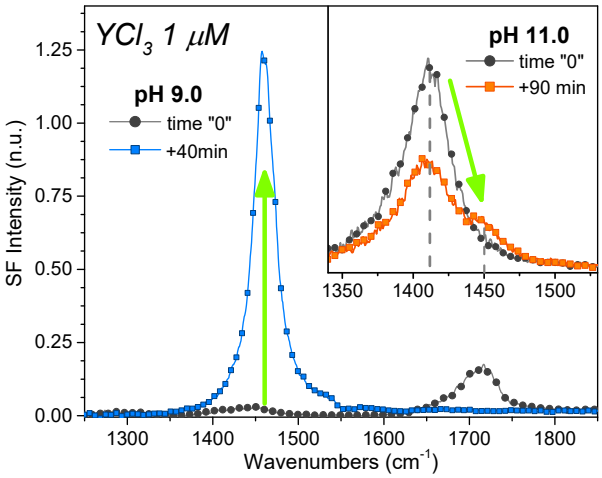

Figure 8. VSF spectra of dAA on 1 μM YCl_3 electrolyte solution at pH 9 and pH 11 (inset), directly after the deposition of the monolayer, and after a time of exposure (+40 min, +90 min).

The time dependence can originate from a diffusion limiting process. The charging of the fatty acid monolayer at high pH generates a negative surface potential that will attract cations to the interface. Although most of the yttrium species in the bulk at pH 9 and pH 11 should be in the hydrated hydroxide form $Y(OH)_{3(s)}$, sub-nanomolar concentrations of the ionic species $Y(OH)^{2+}$, $Y(OH)_2^{+}$, and particularly Y^{3+}, remain in solution (see SI for an extended speciation diagram). Given the low concentrations, the diffusion of such species from the bulk solution to the interface will require some time. Moreover, since the hydronium ion concentration at the surface is a few orders of magnitude higher than in the bulk,[47, 82] the speciation of yttrium in the surface region will also vary, with the preference to eventually form the free Y^{3+} ion. Consequently, diffusion and reaction kinetics will be time-limiting factors.

A time dependence behaviour was also observed in acidic conditions (i.e. pH=5), when almost all yttrium in solution is found in its Y^{3+} form, and ion diffusion to the surface is not the determining factor. In such a case, the underlying cause lies in the state of the monolayer deprotonation, as it is essentially fully uncharged in the absence of trivalent ions in solution (see SI, Figure S6). However, once the monolayer starts to deprotonate upon adsorption of the first ions, the charging accelerates the process. This effect can be used to improve the detection limits of trivalent ions in solution. In the presence of a background monovalent electrolyte (e.g. 100 mM NaCl), the monolayer can partially deprotonate at a lower pH when trivalent ions are more readily found in the free ionic form. For the case of yttrium, we show that the detection limit can be reduced to concentrations below 100 nM (see SI). These results also highlight the importance of carefully considering the potential effects of trace amounts of trivalent ion impurities when studying charged interfaces.[26]

4. Summary and concluding remarks

The carboxylate stretching modes were shown to be sensitive probes for identifying the different types of interactions between the trivalent ions La^{3+} and Y^{3+} and the carboxylic acid moiety. In comparison to the linear IR spectroscopies, the spectral features in VSFS of both the symmetric and asymmetric carboxylate stretches are significantly better resolved, which

simplifies the analysis and interpretation. At least three different carboxylate species could be unambiguously identified when varying the concentration of the trivalent salt in solution. They were linked to both ionic and covalent binding type interactions,[59] with the latter composed primarily of a mixture of bridging and chelating bidentate configurations. This classification, however, relies on a generalized set of rules based on the carboxylate center frequencies, that have several exceptions.[15, 16, 18, 58] In this regard, the results presented in this paper will be useful to extend current theoretical and simulations studies, as well as liquid surface X-ray studies, of polyvalent ions binding structures at the liquid/vapor interface.[57, 83, 84]

Although the same carboxylate species were identified for La^{3+} and Y^{3+}, they show different concentration dependence. In the case of yttrium, once the monolayer is completely deprotonated at ~5 μM, the proportion between the three different carboxylate species remains approximately constant. In contrast, for La^{3+} the relative proportions continue to vary until 10 mM, where the chelating bidentate configuration reaches a maximum at the expense of the ionic contribution, which is no longer detectable at the highest salt concentrations. The difference is ascribed to the almost 20% larger ion size of La^{3+},[67] which provides additional flexibility for finding the most energetically favourable binding pattern.

The specific interactions of Y^{3+} and La^{3+} with the carboxylic acid monolayer lead to charge overcompensation at the surface. Classical electrostatic theories such as the GC theory fail to predict such phenomena, which confirms that specific molecular interactions dominate at the close vicinity of the chemical headgroup, and strongly depend on the nature, electronic structures, and radius of the ions. The charge reversal upon addition of YCl_3 was detected above 10 μM by following the response from water molecules in the interfacial region, which was consistent with the surface pressure isotherms dependence with concentration. The reversal was further supported by the detection of an yttrium hydroxide complex at the surface. The result also highlights the importance of ion speciation in the interfacial region, which due to variations in the concentration of H_3O^+ or OH^- close to the charged interface, it can differ significantly from that in the bulk.

Finally, interactions between Y^{3+} and La^{3+} and the carboxylate headgroup could be detected from concentrations as low as 300 nM in solution. The detection limit was further reduced below 100 nM in the presence of a background electrolyte (i.e. NaCl) that promoted the partial deprotonation of the monolayer. It is anticipated that other trivalent ions known to experience even stronger interactions with the carboxylate moiety, including, among others Co^{3+}, Mn^{3+}, Cr^{3+}, Fe^{3+} or Sc^{3+},[85] could bring the detections limits down to sub nM concentrations. These results strongly indicate that trace amounts of trivalent ions in biological matrices and complex electrolytes could easily dominate the electrolyte interactions with the carboxylic acid moiety.

Electronic Supporting Information (ESI) Available: Langmuir isotherms of AA and dAA on $LaCl_3$ and YCl_3 solutions at various concentrations and pH, details of the fitting procedure of the VSF spectra, predictions from the Gouy-Chapman model, estimation of proportions of metal-carboxylates contributions, VSF spectra showing improved detection limits in the presence of 100 mM NaCl background electrolyte, correlation between symmetric and asymmetric carboxylate stretches, detailed speciation diagrams for YCl_3 and $LaCl_3$, and coarse

modelling of the trivalent ion adsorption on the fatty acid monolayer for the charge compensated case.

Acknowledgements

A.S., S.S, R.C and E.T. acknowledge financial support from Swedish Foundation for Strategic Research (SSF-FFL-5 program), and the Swedish Research Council (VR). E.M.A. and H.C.A. acknowledge funding from The Ohio State University Allen Research Fund and the DOE-BES grant DFXXX, respectively.

Authors present addresses

- ✓ Ellen M. Adams: Department of Physical Chemistry II, Ruhr-Universität Bochum, 44801 Bochum, Germany.
- ✓ Sanghamitra Sengupta. Ultrafast Spectroscopy, AMOLF, 1098 XG Science Park, Amsterdam, The Netherlands.

References

[1] K.D. Collins, Ions from the Hofmeister Series and Osmolytes: Effects on Proteins in Solution and in the Crystallization Process, Methods 34(3) (2004) 300-311.

[2] B.J. Finlayson-Pitts, J.N. Pitts Jr, Chemistry of the Upper and Lower Atmosphere: Theory, Experiments, and Applications, Elsevier1999.

[3] D. Langmuir, Aqueous Environmental, Geochemistry Prentice Hall: Upper Saddle River, NJ (1997).

[4] M. Linden, J.B. Rosenholm, Influence of multivalent metal ions on the monolayer and multilayer properties of some unsaturated fatty acids, Langmuir 11(11) (1995) 4499-4504.

[5] A. Aroti, E. Leontidis, E. Maltseva, G. Brezesinski, Effects of Hofmeister anions on DPPC Langmuir monolayers at the air− water interface, The Journal of Physical Chemistry B 108(39) (2004) 15238-15245.

[6] P. Garidel, A. Blume, 1,2-Dimyristoyl-sn-glycero-3-phosphoglycerol (DMPG) monolayers: influence of temperature, pH, ionic strength and binding of alkaline earth cations, Chemistry and Physics of Lipids 138(1) (2005) 50-59.

[7] V.L. Shapovalov, G. Brezesinski, Breakdown of the Gouy−Chapman Model for Highly Charged Langmuir Monolayers: Counterion Size Effect, The Journal of Physical Chemistry B 110(20) (2006) 10032-10040.

[8] A. Cordomí, O. Edholm, J.J. Perez, Effect of Ions on a Dipalmitoyl Phosphatidylcholine Bilayer. A Molecular Dynamics Simulation Study, The Journal of Physical Chemistry B 112(5) (2008) 1397-1408.

[9] S. Kewalramani, H. Hlaing, B.M. Ocko, I. Kuzmenko, M. Fukuto, Effects of Divalent Cations on Phase Behavior and Structure of a Zwitterionic Phospholipid (DMPC) Monolayer at the Air−Water Interface, The Journal of Physical Chemistry Letters 1(2) (2010) 489-495.

[10] C.E. McNamee, M. Kappl, H.-J. Butt, J. Ally, H. Shigenobu, Y. Iwafuji, K. Higashitani, K. Graf, Forces between a monolayer at an air/water interface and a particle in solution: influence of the sign of the surface charges and the subphase salt concentration, Soft Matter 7(21) (2011) 10182-10192.

[11] E.M. Adams, C.B. Casper, H.C. Allen, Effect of cation enrichment on dipalmitoylphosphatidylcholine (DPPC) monolayers at the air-water interface, Journal of Colloid and Interface Science 478 (2016) 353-364.

[12] H. Tervahattu, J. Juhanoja, K. Kupiainen, Identification of an Organic Coating on Marine Aerosol Particles by TOF-SIMS, Journal of Geophysical Research: Atmospheres 107(D16) (2002) ACH 18-1-ACH 18-7.
[13] A.A. Spector, Essentiality of Fatty Acids, Lipids 34 (1999) S1-S3.
[14] R.E. Cochran, O. Laskina, T. Jayarathne, A. Laskin, J. Laskin, P. Lin, C. Sultana, C. Lee, K.A. Moore, C.D. Cappa, Analysis of Organic Anionic Surfactants in Fine and Coarse Fractions of Freshly Emitted Sea Spray Aerosol, Environmental science & technology 50(5) (2016) 2477-2486.
[15] G.B. Deacon, R.J. Phillips, Relationships between the carbon-oxygen stretching frequencies of carboxylato complexes and the type of carboxylate coordination, Coord. Chem. Rev. 33(3) (1980) 227-250.
[16] G.B. Deacon, F. Huber, R.J. Phillips, Diagnosis of the Nature of Carboxylate Coordination from the Direction of Shifts of Carbon - Oxygen Stretching Frequencies, Inorganica Chimica Acta 104(1) (1985) 41-45.
[17] A. Ouchi, Y. Suzuki, Y. Ohki, Y. Koizumi, Structure of Rare Earth Carboxylates in Dimeric and Polymeric Forms, Coordination Chemistry Reviews 92 (1988) 29-43.
[18] J.E. Tackett, FT-IR Characterization of Metal Acetates in Aqueous Solution, Appl. Spectrosc. 43(3) (1989) 483-489.
[19] J. Kmetko, A. Datta, G. Evmenenko, P. Dutta, The Effects of Divalent Ions on Langmuir Monolayer and Subphase Structure: A Grazing-Incidence Diffraction and Bragg Rod Study, The Journal of Physical Chemistry B 105(44) (2001) 10818-10825.
[20] A. Gericke, H. Hühnerfuss, The effect of cations on the order of saturated fatty acid monolayers at the air-water interface as determined by infrared reflection-absorption spectrometry, Thin Solid Films 245(1) (1994) 74-82.
[21] J. Simon-Kutscher, A. Gericke, H. Hühnerfuss, Effect of Bivalent Ba, Cu, Ni, and Zn Cations on the Structure of Octadecanoic Acid Monolayers at the Air−Water Interface As Determined by External Infrared Reflection−Absorption Spectroscopy, Langmuir 12(4) (1996) 1027-1034.
[22] C.Y. Tang, Z. Huang, H.C. Allen, Binding of Mg^{2+} and Ca^{2+} to Palmitic Acid and Deprotonation of the COOH Headgroup Studied by Vibrational Sum Frequency Generation Spectroscopy, J. Phys. Chem. B 114(51) (2010) 17068-17076.
[23] E.J. Robertson, D.K. Beaman, G.L. Richmond, Designated Drivers: The Differing Roles of Divalent Metal Ions in Surfactant Adsorption at the Oil–Water Interface, Langmuir 29(50) (2013) 15511-15520.
[24] Z. Huang, W. Hua, D. Verreault, H.C. Allen, Influence of Salt Purity on Na^{+} and Palmitic Acid Interactions, The Journal of Physical Chemistry A 117(50) (2013) 13412-13418.
[25] M. Scott, Interactions of Divalent Cations with the Carboxylate Moiety : A Vibrational Sum Frequency Study, KTH Royal Institute of Technology, 2018, p. 91.
[26] A. Sthoer, J. Hladilkova, M. Lund, E. Tyrode, Molecular insight into carboxylic acid - alkali metal cations interactions: reversed affinities and ion-pair formation revealed by non-linear optics and simulations, Phys. Chem. Chem. Phys 21 (2019) 11329-11344.
[27] W. Hua, D. Verreault, E.M. Adams, Z. Huang, H.C. Allen, Impact of Salt Purity on Interfacial Water Organization Revealed by Conventional and Heterodyne-Detected Vibrational Sum Frequency Generation Spectroscopy, The Journal of Physical Chemistry C 117(38) (2013) 19577-19585.
[28] M.E. Richert, G.G. Gochev, B. Braunschweig, Specific Ion Effects of Trivalent Cations on the Structure and Charging State of β-Lactoglobulin Adsorption Layers, Langmuir 35(35) (2019) 11299-11307.

[29] F. Roosen-Runge, B.S. Heck, F. Zhang, O. Kohlbacher, F. Schreiber, Interplay of pH and Binding of Multivalent Metal Ions: Charge Inversion and Reentrant Condensation in Protein Solutions, The Journal of Physical Chemistry B 117(18) (2013) 5777-5787.
[30] M.R. Fries, N.F. Conzelmann, L. Günter, O. Matsarskaia, M.W.A. Skoda, R.M.J. Jacobs, F. Zhang, F. Schreiber, Bulk Phase Behavior vs Interface Adsorption: Specific Multivalent Cation and Anion Effects on BSA Interactions, Langmuir 37(1) (2021) 139-150.
[31] W. Wang, W. Bu, L. Wang, P.E. Palo, S. Mallapragada, M. Nilsen-Hamilton, D. Vaknin, Interfacial Properties and Iron Binding to Bacterial Proteins That Promote the Growth of Magnetite Nanocrystals: X-ray Reflectivity and Surface Spectroscopy Studies, Langmuir 28(9) (2012) 4274-4282.
[32] J. Schubert, C. Radeke, A. Fery, M. Chanana, The role of pH, metal ions and their hydroxides in charge reversal of protein-coated nanoparticles, Physical Chemistry Chemical Physics (2019).
[33] J. Pittler, W. Bu, D. Vaknin, A. Travesset, D.J. McGillivray, M. Lösche, Charge Inversion at Minute Electrolyte Concentrations, Physical Review Letters 97(4) (2006) 046102.
[34] M.M. Sartin, W. Sung, S. Nihonyanagi, T. Tahara, Molecular mechanism of charge inversion revealed by polar orientation of interfacial water molecules: A heterodyne-detected vibrational sum frequency generation study, The Journal of Chemical Physics 149(2) (2018) 024703.
[35] W. Wang, R.Y. Park, D.H. Meyer, A. Travesset, D. Vaknin, Ionic Specificity in pH Regulated Charged Interfaces: Fe^{3+}versus La^{3+}, Langmuir 27(19) (2011) 11917-11924.
[36] W. Wang, R.Y. Park, A. Travesset, D. Vaknin, Ion-Specific Induced Charges at Aqueous Soft Interfaces, Phys. Rev. Lett. 106(5) (2011) 056102.
[37] N.T. Hue, N.A. Tuan, Interaction of arachidic acid langmuir monolayers with trivalent ions La^{3+} and Fe^{3+} studied by vibrational sum-frequency spectroscopy, Materials Transactions 59(7) (2018) 1087-1090.
[38] W. Sung, S. Krem, D. Kim, Binding of trivalent ions on fatty acid Langmuir monolayer: Fe^{3+} versus La^{3+}, J. Chem. Phys. 149(16) (2018) 163304.
[39] K. Binnemans, Lanthanide-Based Luminescent Hybrid Materials, Chemical Reviews 109(9) (2009) 4283-4374.
[40] D.J. Johnson, D.T. Amm, T. Laursen, S.K. Gupta, Langmuir-Blodgett deposition of yttrium arachidate, Thin Solid Films 232(2) (1993) 245-251.
[41] J.F.D. Liljeblad, E. Tyrode, Vibrational Sum Frequency Spectroscopy Studies at Solid/Liquid Interfaces: Influence of the Experimental Geometry in the Spectral Shape and Enhancement, J. Phys. Chem. C 116(43) (2012) 22893-22903.
[42] C.D. Bain, P.B. Davies, T.H. Ong, R.N. Ward, M.A. Brown, Quantitative Analysis of Monolayer Composition by Sum-Frequency Vibrational Spectroscopy, Langmuir 7(8) (1991) 1563-1566.
[43] L. Dalstein, E. Potapova, E. Tyrode, The elusive silica/water interface: isolated silanols under water as revealed by vibrational sum frequency spectroscopy, Phys. Chem. Chem. Phys 19(16) (2017) 10343-10349.
[44] G.L. Gaines, Insoluble Monolayers at Liquid-Gas Interfaces, Wiley Interscience, New York, 1966.
[45] R.M. Kenn, C. Boehm, A.M. Bibo, I.R. Peterson, H. Moehwald, J. Als-Nielsen, K. Kjaer, Mesophases and Crystalline Phases in Fatty Acid Monolayers, The Journal of Physical Chemistry 95(5) (1991) 2092-2097.
[46] V.M. Kaganer, H. Möhwald, P. Dutta, Structure and phase transitions in Langmuir monolayers, Rev. Mod. Phys. 71(3) (1999) 779-819.

[47] E. Tyrode, R. Corkery, Charging of Carboxylic Acid Monolayers with Monovalent Ions at Low Ionic Strengths: Molecular Insight Revealed by Vibrational Sum Frequency Spectroscopy, J. Phys. Chem. C 122(50) (2018) 28775-28786.
[48] E.D. Goddard, O. Kao, H.C. Kung, Monolayer properties of fatty acids: IV. Influence of cation at high pH, J. Colloid Interface Sci. 24(3) (1967) 297-309.
[49] H.S. Rivière S., Meunier J., Schwarz D. K., Tsao M. W., Knobler C. M., Textures and Phase Transitions in Langmuir Monolayers of Fatty Acids. A Comparative Brewster Angle Microscope and Polarized Fluorescence Microscope Study, The Journal of Chemical Physics 101(11) (1994) 10045-10051.
[50] A. Angelova, D. Vollhardt, R. Ionov, 2D−3D Transformations of Amphiphilic Monolayers Influenced by Intermolecular Interactions: A Brewster Angle Microscopy Study, The Journal of Physical Chemistry 100(25) (1996) 10710-10720.
[51] Y. Oishi, Y. Takashima, K. Suehiro, T. Kajiyama, Effect of Ionic Repulsion among Hydrophilic Groups on Aggregation Structure of Fatty Acid Monolayer on the Water Surface, Langmuir 13(9) (1997) 2527-2532.
[52] S. Kundu, D. Langevin, Fatty acid monolayer dissociation and collapse: Effect of pH and cations, Colloids and Surfaces A: Physicochemical and Engineering Aspects 325(1) (2008) 81-85.
[53] V.B. Fainerman, D. Vollhardt, R. Johann, Arachidic Acid Monolayers at High pH of the Aqueous Subphase: Studies of Counterion Bonding, Langmuir 16(20) (2000) 7731-7736.
[54] A. Sthoer, E. Tyrode, Interactions of Na^+ Cations with a Highly Charged Fatty Acid Langmuir Monolayer: Molecular Description of the Phase Transition, J. Phys. Chem. C 123 (2019) 23037−23048.
[55] E. Tyrode, J. Hedberg, A Comparative Study of the CD and CH Stretching Spectral Regions of Typical Surfactants Systems Using VSFS: Orientation Analysis of the Terminal CH_3 and CD_3 Groups, J. Phys. Chem. C 116(1) (2012) 1080-1091.
[56] K. Nakamoto, J. Fujita, S. Tanaka, M. Kobayashi, Infrared Spectra of Metallic Complexes. IV. Comparison of the Infrared Spectra of Unidentate and Bidentate Metallic Complexes, Journal of the American Chemical Society 79(18) (1957) 4904-4908.
[57] J.K. Denton, P.J. Kelleher, M.A. Johnson, M.D. Baer, S.M. Kathmann, C.J. Mundy, B.A. Wellen Rudd, H.C. Allen, T.H. Choi, K.D. Jordan, Molecular-level origin of the carboxylate head group response to divalent metal ion complexation at the air–water interface, Proc. Natl. Acad. Sci. 116(30) (2019) 14874-14880.
[58] B. Manhas, A. Trikha, Relationships between the direction of shifts in the carbon-oxygen stretching frequencies of carboxylato complexes and the type of carboxylate coordination, J.Indian Chem 54 (1982) 315-321.
[59] Y. Marcus, G. Hefter, Ion Pairing, Chem. Rev. 106(11) (2006) 4585-4621.
[60] F. Ribot, P. Toledano, C. Sanchez, X-ray and Spectroscopic Investigations of the Structure of Yttrium Acetate Tetrahydrate, Inorganica Chimica Acta 185(2) (1991) 239-245.
[61] T. Takekiyo, Y. Yoshimura, Raman Study of the Coordination Structure of a Rare Earth−Acetate Complex in Water, The Journal of Physical Chemistry A 111(27) (2007) 6039-6043.
[62] K. Binnemans, L. Jongen, C. Bromant, D. Hinz, G. Meyer, Structure and Mesomorphism of Neodymium(III) Alkanoates, Inorganic Chemistry 39(26) (2000) 5938-5945.
[63] L. Jongen, G. Meyer, K. Binnemans, Crystal structure of lanthanum(III) butyrate monohydrate, Journal of Alloys and Compounds 323-324 (2001) 142-146.
[64] R.W. Corkery, Metal Organic Framework (MOF) Liquid Crystals. 1D, 2D and 3D Ionic Coordination Polymer Structures in the Thermotropic Mesophases of Metal Soaps, Including Alkaline Earth, Transition Metal and Lanthanide Soaps, Current Opinion in Colloid & Interface Science 13(4) (2008) 288-302.

[65] L. Ciontea, M. Nasui, T. Petrisor, R.B. Mos, M.S. Gabor, R.A. Varga, T. Petrisor, Synthesis, crystal structure and thermal decomposition of [La2(CH3CH2COO)6·(H2O)3]·3.5H2O precursor for high-k La2O3 thin films deposition, Materials Research Bulletin 45(9) (2010) 1203-1208.
[66] I.A. Martynova, D.M. Tsymbarenko, N.P. Kuz'mina, Yttrium tris-propionate monohydrate: Synthesis, crystal structure, and thermal stability, Russian Journal of Coordination Chemistry 40(8) (2014) 565-570.
[67] R. Shannon, Revised effective ionic radii and systematic studies of interatomic distances in halides and chalcogenides, Acta Crystallographica Section A 32(5) (1976) 751-767.
[68] G. Gonella, C. Lütgebaucks, A.G.F. de Beer, S. Roke, Second Harmonic and Sum-Frequency Generation from Aqueous Interfaces Is Modulated by Interference, J. Phys. Chem. C 120(17) (2016) 9165-9173.
[69] Y.-C. Wen, S. Zha, X. Liu, S. Yang, P. Guo, G. Shi, H. Fang, Y.R. Shen, C. Tian, Unveiling Microscopic Structures of Charged Water Interfaces by Surface-Specific Vibrational Spectroscopy, Phys. Rev. Lett. 116(1) (2016) 016101.
[70] S.K. Reddy, R. Thiraux, B.A. Wellen Rudd, L. Lin, T. Adel, T. Joutsuka, F.M. Geiger, H.C. Allen, A. Morita, F. Paesani, Bulk Contributions Modulate the Sum-Frequency Generation Spectra of Water on Model Sea-Spray Aerosols, Chem 4(7) (2018) 1629-1644.
[71] D.K. Hore, E. Tyrode, Probing Charged Aqueous Interfaces Near Critical Angles: Effect of Varying Coherence Length, J. Phys. Chem. C 123 (2019) 16911-16920.
[72] E. Tyrode, M.W. Rutland, C.D. Bain, Adsorption of CTAB on Hydrophilic Silica Studied by Linear and Nonlinear Optical Spectroscopy, J. Am. Chem. Soc. 130(51) (2008) 17434-17445.
[73] S.C. Flores, J. Kherb, P.S. Cremer, Direct and Reverse Hofmeister Effects on Interfacial Water Structure, The Journal of Physical Chemistry C 116(27) (2012) 14408-14413.
[74] K.A. Becraft, F.G. Moore, G.L. Richmond, In-situ spectroscopic investigations of surfactant adsorption and water structure at the CaF2/aqueous solution interface, Physical Chemistry Chemical Physics 6(8) (2004) 1880-1889.
[75] D. Lis, E.H.G. Backus, J. Hunger, S.H. Parekh, M. Bonn, Liquid flow along a solid surface reversibly alters interfacial chemistry, Science 344(6188) (2014) 1138-1142.
[76] D.F. Evans, H. Wennerström, The Colloidal Domain: Where Physics, Chemistry, Biology, and Technology Meet, 2nd, 1998.
[77] J. Lyklema, Overcharging, Charge Reversal: Chemistry or Physics?, Colloids and Surfaces A: Physicochemical and Engineering Aspects 291(1) (2006) 3-12.
[78] E. Wernersson, R. Kjellander, J. Lyklema, Charge Inversion and Ion−Ion Correlation Effects at the Mercury/Aqueous MgSO4 Interface: Toward the Solution of a Long-Standing Issue, J. Phys. Chem. C 114(4) (2010) 1849-1866.
[79] M. Rashwan, B. Rehl, A. Sthoer, A.M. Darlington, M.S. Azam, H. Zeng, Q. Liu, E. Tyrode, J.M. Gibbs, Structure of the Silica/Divalent Electrolyte Interface: Molecular Insight into Charge Inversion with Increasing pH, J. Phys. Chem. C 124(49) (2020) 26973-26981.
[80] L. Zhang, C. Tian, G.A. Waychunas, Y.R. Shen, Structures and Charging of α-Alumina (0001)/Water Interfaces Studied by Sum-Frequency Vibrational Spectroscopy, Journal of the American Chemical Society 130(24) (2008) 7686-7694.
[81] K.A. Becraft, G.L. Richmond, In Situ Vibrational Spectroscopic Studies of the CaF2/H2O Interface, Langmuir 17(25) (2001) 7721-7724.
[82] E. Tyrode, S. Sengupta, A. Sthoer, Identifying Eigen-like hydrated protons at negatively charged interfaces, Nat. Commun. 11(1) (2020) 493.
[83] W. Bu, M.L. Schlossman, Synchrotron X-Ray Scattering from Liquid Surfaces and Interfaces, in: E.J. Jaeschke, S. Khan, J.R. Schneider, J.B. Hastings (Eds.), Synchrotron

Light Sources and Free-Electron Lasers: Accelerator Physics, Instrumentation and Science Applications, Springer International Publishing, Cham, 2020, pp. 1897-1933.
[84] A. Uysal, W. Rock, B. Qiao, W. Bu, B. Lin, Two-Step Adsorption of $PtCl_6^{2-}$ Complexes at a Charged Langmuir Monolayer: Role of Hydration and Ion Correlations, J. Phys. Chem. C 121(45) (2017) 25377-25383.
[85] D.C. Harris, C.A. Lucy, H. University of North Carolina at Chapel, C. Department of, Quantitative chemical analysis, Freeman Custom Publishing, New York, NY, 2016.